Impact of scanning velocity on microstructure and mechanical properties of Inconel 738LC alloys fabricated by laser powder bed fusion

Yixuan Chen[1],Weihao Wang[1]; Yao Ou[1]; Yingna Wu[1]; Zirong Zhai†[1]; Rui Yang[1,2];
[1]Center for Adaptive System Engineering, School of Creativity and Arts, Shanghaitech University, No.393 Middle Huaxia Road, Pudong, Shanghai, 201210
[2]Institute of Metal Research, Chinese Academy of Sciences, No.72 Wenhua Road, Shenyang, Liaoning, 110016

Objectives

1. Compare the melt pool morphology, microstructure and mechanical properties of L-PBFed Inconel738LC parts based on the same volumetric energy density but distinct laser power and scanning velocity
2. Investigate the influences of laser power and scanning speed on the microstructure and mechanical property of Inconel738LC fabricated by LPBF, and make the explanation by using physical model.

Background

1. Inconel 738LC is a typical nickel-based gamma-prime (γ') precipitation-strengthened superalloy. It has excellent corrosion and oxidation resistance and good creep properties at elevated temperatures. The high-temperature properties of Inconel 738LC alloy strongly depend on the γ' ($Ni_3(Al, Ti)$) phase precipitation. However, the total amount of Al and Ti in its composition is above 7 wt%, which leads to poor weldability.
2. Many researchers have focused on cracking mitigating by process optimizations [4, 5]. Although some researches have achieved the proper process window of LPBF-ed Inconel 738LC based on different volumetric/linear energy densities, the deep mechanism beyond formalized energy density of the effects of laser power and scanning speed are still not fully discussed.

Material and methods

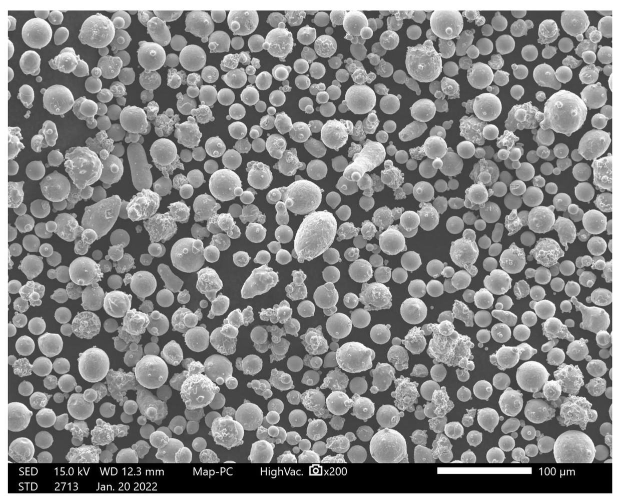

Fig1. SEM image of the Inconel 738LC powder (D10=16.5 μm, D50=27.3 μm, and D90=44.3 μm)

Volumetric energy density:

$$ED = \frac{P}{vHt}$$

P: laser power, v: scanning speed, H: hatch spacing, t: layer thickness (t = 30 μm)

Alloy	Cr	Co	Mo	W	Al	Ti	Ta	Nb	C	B	Zr
Inconel 738LC	16.0	8.5	1.75	2.6	3.4	3.4	1.75	0.9	0.11	0.01	0.04

Table 1. The chemical compositions (in weight%) of Inconel 738LC

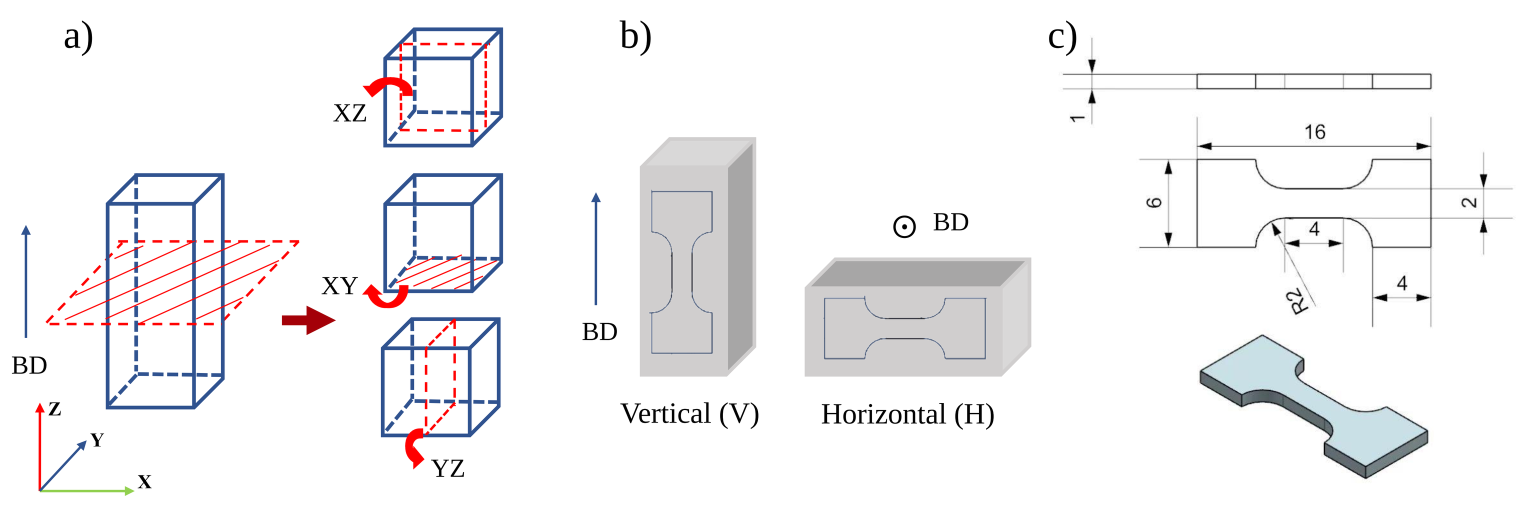

Fig 2. a) Observation section in three directions, b) The schematic maps of as-built Inconel 738LC blocks in two directions (parallel or perpendicular to the building direction), c) tensile specimen CAD graphics.

	Power(W)	Scanning speed(mm/s)	Hatching(mm)	Energy density(J/mm³)
1	100	600		
2	175	1050	0.1	55.56
3	250	1500		

Table 2. Processing parameter sets of SLM Inconel 738LC

Mechanical properties

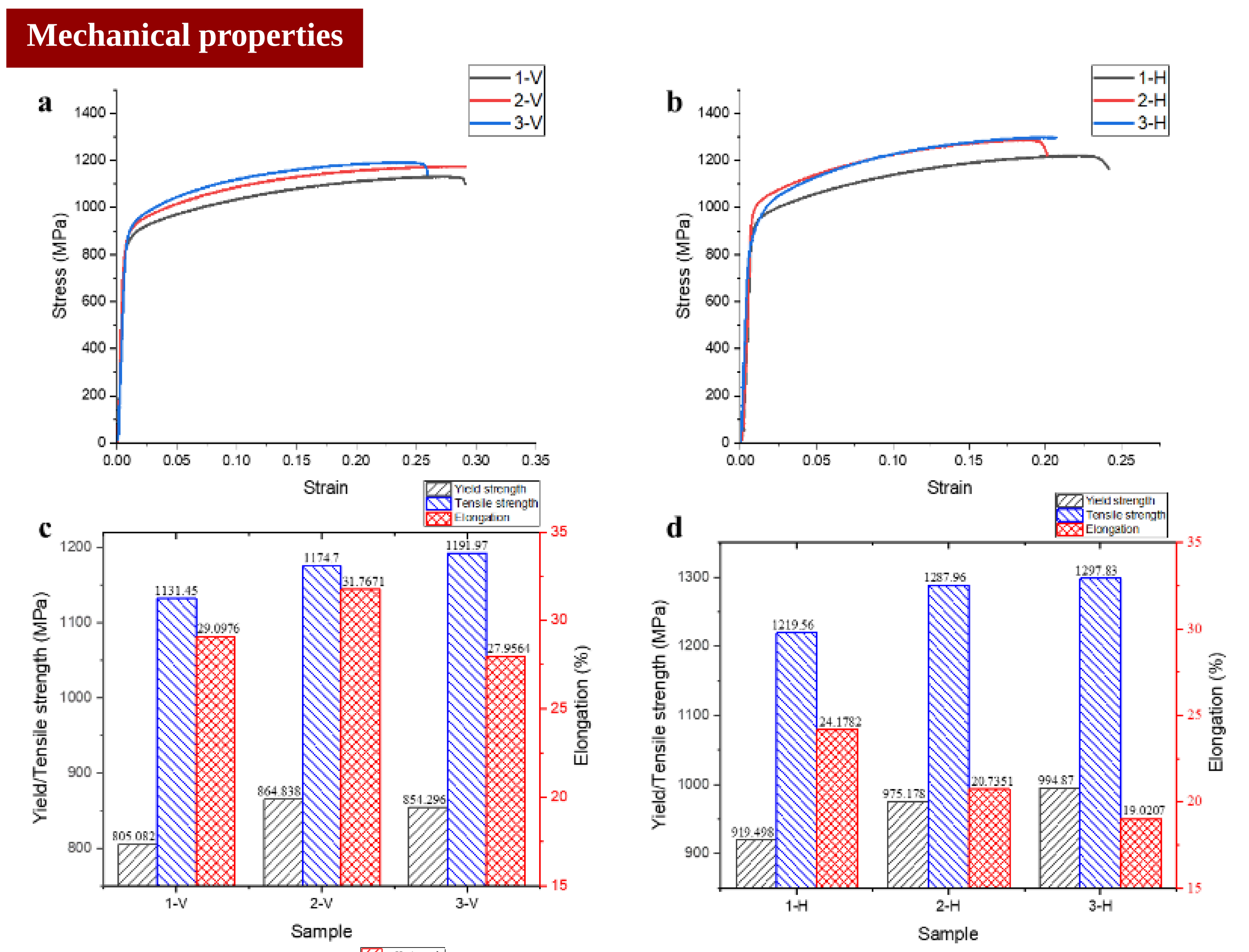

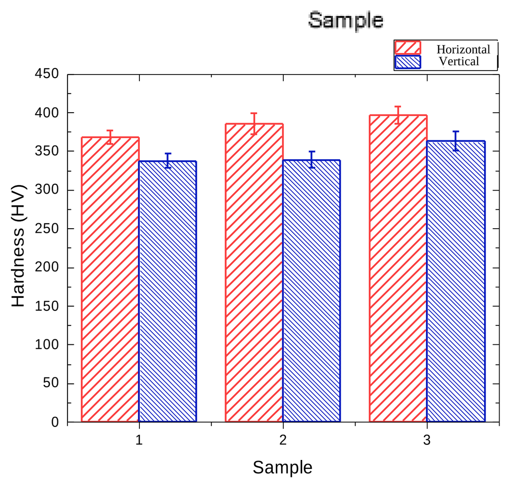

Fig 6. a) stress-strain curves of vertical sample specimen, b) stress-strain curves of horizontal sample specimen, c) tensile testing results of vertical sample specimen, d) tensile testing results of horizontal sample specimen

Fig 7. Vickers hardness of three different building parameters samples of 1#, 2# and 3#

Melt pool morphology analysis

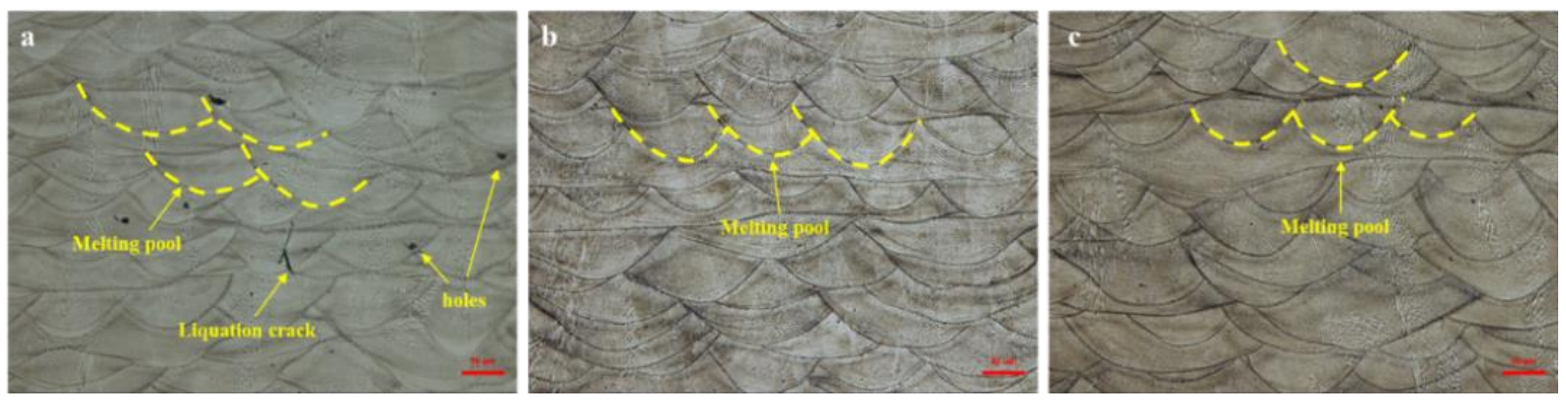

Fig 3. OM results of a) sample 1# (100W, 600mm/s), b) sample 2# (175W, 1050mm/s), c) sample 3# (250W, 2500mm/s) from XZ transactions (along the building direction)

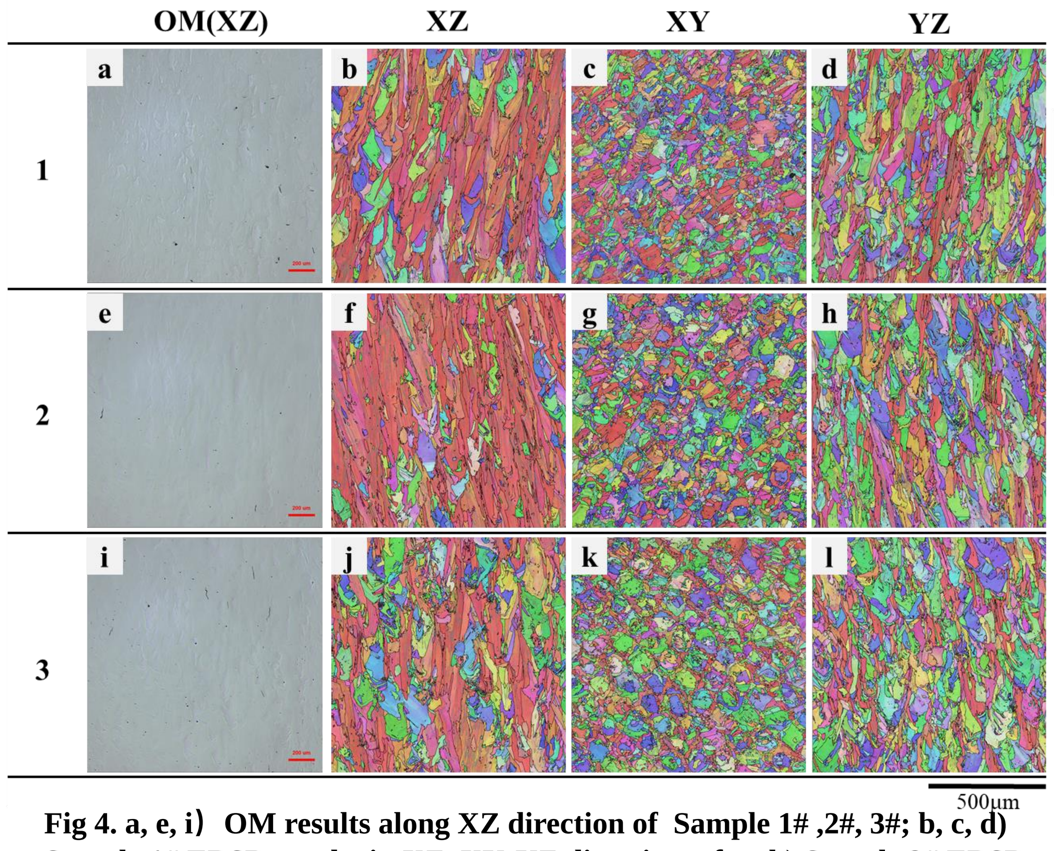

Fig 4. a, e, i） OM results along XZ direction of Sample 1# ,2#, 3#; b, c, d) Sample 1# EBSD results in XZ, XY, YZ directions; f, g, h) Sample 2# EBSD results in XZ, XY, YZ directions; j, k, l) Sample 3# EBSD results in XZ, XY, YZ directions.

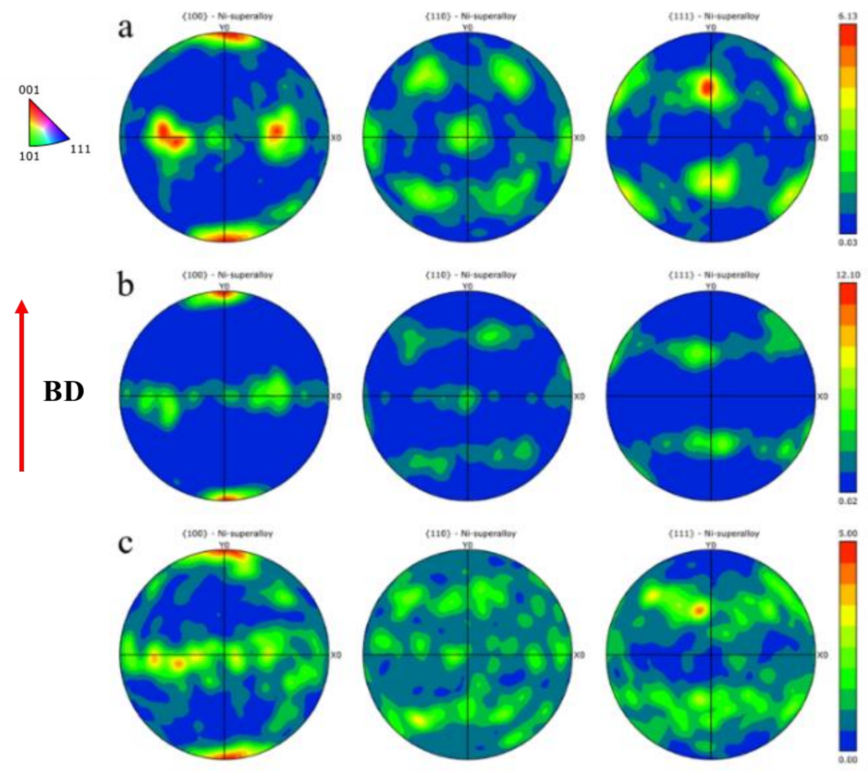

Fig 5. Pole figures of a) Sample 1#, b) Sample 2#, c) Sample 3# along XZ direction

Sample	Grain boundary fraction(%) Small angle boundary (2-15°)	Grain boundary fraction(%) Large angle boundary (>15°)	Grain size (μm)	Recrystallization grains fraction (%)
1-XY	40.5	59.5	13.56±11.65	28.2
2-XY	30.1	69.9	13.48±11.88	31.3
3-XY	28.6	71.4	11.64±10.32	39.9
1-XZ	41.1	58.6	16.41±17.14	26.3
2-XZ	35.8	64.2	15.39±16.59	27.9
3-XZ	28.5	71.5	14.53±14.98	33.0
1-YZ	52.2	47.8	20.06±27.17	13.3
2-YZ	50.0	50.0	17.10±25.13	20.1
3-YZ	36.8	63.2	14.49±18.14	23.3

Table 4. The EBSD results illustrate the distinctions among sample1#,2# and 3#

1. The fraction of low angle grain boundary (LAGB) and the grain size decreases when the laser power and scanning speed increasing along XY, XZ, or YZ direction. On the contrary, the fraction of recrystallized grains shows a completely reverse trend
2. The average grain size in the XY direction is slightly smaller than that in the other two directions, mainly led by the higher cooling rate along the XY direction.
3. Sample 2# in the XZ direction has the strongest texture, and the primary texture type of sample 1 is GOSS texture of {1 1 0} <0 0 1>; Many hybrid crystals in sample 3# are distributed in different positions of the pole figure

CFD simulation

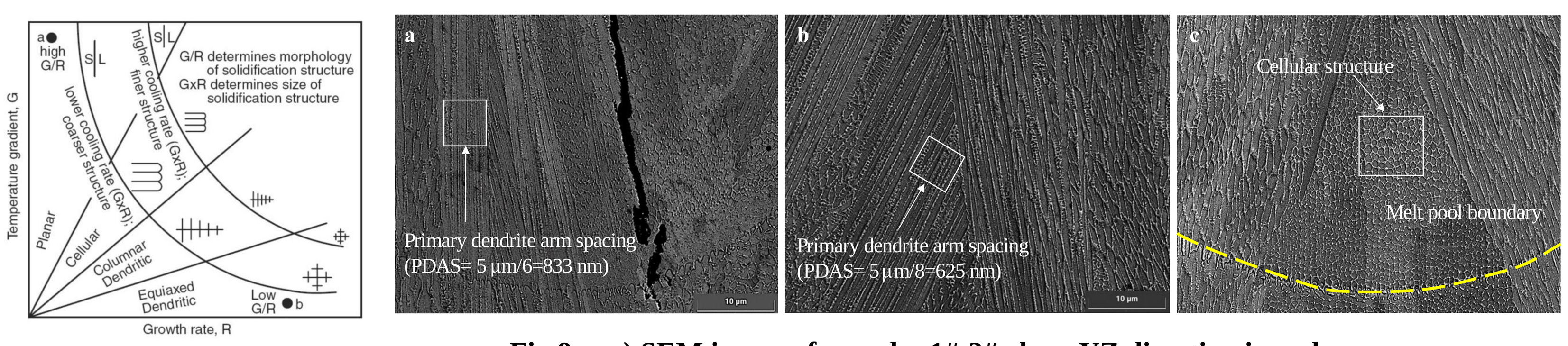

Fig 8. a-c) SEM image of samples 1#-3# along YZ direction in order

The cooling rate at the bottom of the melt pool in sample 3# is higher than other positions in the melt pool, while the cooling rates at different positions of the melt pool only have a relatively slight difference in sample 1#.

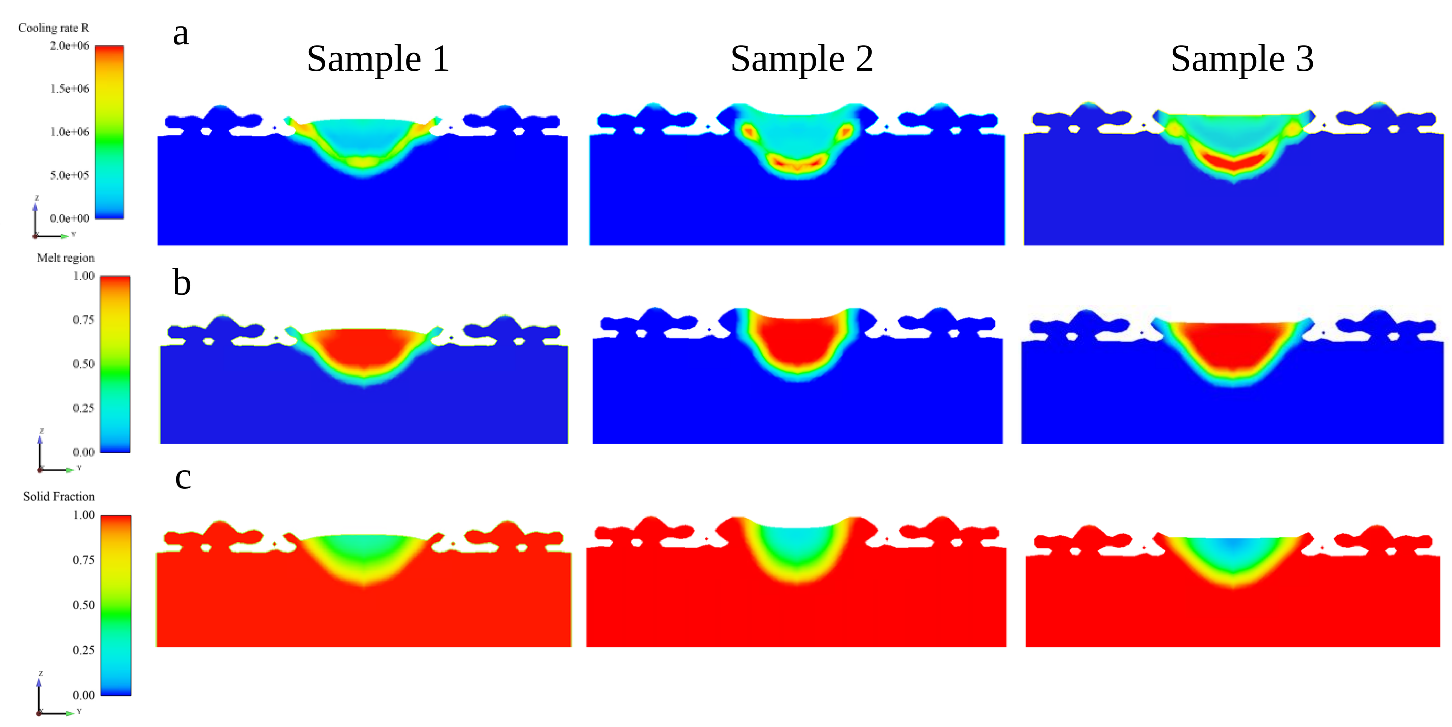

Fig 9. CFD simulation results of melt pool in YZ, a) cooling rate, b) melt region, c) solid fraction

Conclusions

1) Different combinations of laser power and scanning velocity can produce distinct microstructures and tensile behavior caused by the diverse thermal history. It is noteworthy that the building parameter of high scanning speed and high power produces a wider melt pool with a higher cooling rate than the one of low scanning speed and low powder.
2) Relatively highest YS and UTS can be achieved in the case of high power with high-speed scanning velocity due to dislocation strengthen caused by the high-temperature gradient.

References

1. Perevoshchikova, et al., *Optimisation of selective laser melting parameters for the Ni-based superalloy IN-738 LC using Doehlert's design.* Rapid Prototyping Journal, 2017.
2. Zhang, L., et al., *Selective laser melting of IN738 superalloy with a low Mn+Si content: Effect of energy input on characteristics of molten pool, metallurgical defects, microstructures and mechanical properties.* Materials Science and Engineering: A, 2021. **826**: p. 141985.
3. Reed, R.C., *The Superalloys : Fundamentals and Applications*. 2006, Cambridge, UNITED KINGDOM: Cambridge University Press.
4. Danis, Y., E. Lacoste, and C. Arvieu, *Numerical modeling of inconel 738LC deposition welding: Prediction of residual stress induced cracking.* Journal of Materials Processing Technology, 2010. 210(14): p. 2053-2061.
5. Chapman, L.A., et al., *PAMRIC: Properties of Alloys and Moulds Relevant to Investment Casting*.
6. Aune, R.E., et al., *Thermophysical properties of IN738lc, MM247lc and CMSX-4 in the liquid and high temperature solid phase*. Superalloys 718, 625, 706, 2005: p. 467-476.